EUROPEAN ORGANIZATION FOR NUCLEAR RESEARCH

CERN-EP-2017-xxx
18 July 2017

Systematic studies of correlations between different order flow harmonics in Pb–Pb collisions at $\sqrt{s_{\mathrm{NN}}} = 2.76$ TeV

ALICE Collaboration*

Abstract

The correlations between event-by-event fluctuations of anisotropic flow harmonic amplitudes have been measured in Pb–Pb collisions at $\sqrt{s_{\mathrm{NN}}} = 2.76$ TeV with the ALICE detector at the Large Hadron Collider. The results were obtained with the multiparticle correlation observables dubbed Symmetric Cumulants. These observables are robust against biases originating from nonflow effects. The centrality dependence of correlations between the higher order harmonics (the quadrangular v_4 and pentagonal v_5 flow) and the lower order harmonics (the elliptic v_2 and triangular v_3 flow) is presented. The transverse momentum dependence of correlations between v_3 and v_2 and between v_4 and v_2 is also reported. The results are compared to calculations from viscous hydrodynamics and A Multi-Phase Transport (AMPT) model calculations. The comparisons to viscous hydrodynamic models demonstrate that the different order harmonic correlations respond differently to the initial conditions and the temperature dependence of the ratio of shear viscosity to entropy density (η/s). A small average value of η/s is favored independent of the specific choice of initial conditions in the models. The calculations with the AMPT initial conditions yield results closest to the measurements. Correlations between the magnitudes of v_2, v_3 and v_4 show moderate p_{T} dependence in mid-central collisions. This might be an indication of possible viscous corrections to the equilibrium distribution at hadronic freeze-out, which might help to understand the possible contribution of bulk viscosity in the hadronic phase of the system. Together with existing measurements of individual flow harmonics, the presented results provide further constraints on initial conditions and the transport properties of the system produced in heavy-ion collisions.

*See Appendix B for the list of collaboration members

1 Introduction

The main emphasis of the ultra-relativistic heavy-ion collision programs at the Relativistic Heavy Ion Collider (RHIC) and the Large Hadron Collider (LHC) is to study the deconfined phase of strongly interacting nuclear matter, the Quark-Gluon Plasma (QGP). The matter produced in a heavy-ion collision exhibits strong collective radial expansion. Due to anisotropic pressure gradients in the plane transverse to the beam direction, more particles emitted in the direction of the largest gradients result in anisotropic transverse flow. The large elliptic flow discovered at RHIC energies [1] is also observed at LHC energies [2, 3]. The measurements are well described by calculations utilizing viscous hydrodynamics [4–9]. These calculations also demonstrated that the shear viscosity to the entropy density ratio (η/s) of the QGP in heavy-ion collisions at RHIC and LHC energies is close to a universal lower bound $1/4\pi$ [10].

The temperature dependence of η/s has some generic features that most known fluids obey. One such general behavior is that this ratio typically reaches its minimum value close to the phase transition region [11]. It was shown, using kinetic theory and quantum mechanical considerations [12], that $\eta/s \sim 0.1$ would be the correct order of magnitude for the lowest possible shear viscosity to entropy density ratio value found in nature. Later it was demonstrated that an exact lower bound $(\eta/s)_{\rm min} = 1/4\pi \approx 0.08$ can be conjectured using AdS/CFT correspondence [10]. Hydrodynamical simulations constrained by data support the view that η/s of the QGP is close to that limit [8]. It is argued that such a low value might imply that thermodynamic trajectories for the expanding matter would lie close to the quantum chromodynamics (QCD) critical end point, which is another subject of intensive experimental study [11, 13].

Anisotropic flow [14] is quantified with $n^{\rm th}$-order flow harmonics v_n and corresponding symmetry plane angles Ψ_n in a Fourier decomposition of the particle azimuthal distribution in the plane transverse to the beam direction [15, 16]:

$$E\frac{{\rm d}^3N}{{\rm d}\mathbf{p}^3} = \frac{1}{2\pi}\frac{{\rm d}^2N}{p_{\rm T}{\rm d}p_{\rm T}{\rm d}\eta}\left\{1+2\sum_{n=1}^{\infty} v_n(p_{\rm T},\eta)\cos[n(\varphi-\Psi_n)]\right\}, \tag{1}$$

where E, $\mathbf{p}$, $p_{\rm T}$, φ and η are the particle's energy, momentum, transverse momentum, azimuthal angle and pseudorapidity, respectively, and Ψ_n is the azimuthal angle of the symmetry plane of the $n^{\rm th}$-order harmonic. Harmonic v_n can be calculated as $v_n = \langle\cos[n(\varphi-\Psi_n)]\rangle$, where the brackets denote an average over all particles in all events. The anisotropic flow in heavy-ion collisions is typically understood as the hydrodynamic response of the produced matter to spatial deformations of the initial energy density profile [17]. This profile fluctuates event-by-event due to fluctuating positions of the constituents inside the colliding nuclei, which implies that v_n also fluctuates [18, 19]. The recognition of the importance of flow fluctuations led to the discovery of triangular and higher flow harmonics [20, 21] as well as to the correlations between different v_n harmonics [22, 23]. The higher order harmonics are expected to be sensitive to fluctuations in the initial conditions and to the magnitude of η/s [24, 25], while v_n correlations have the potential to discriminate between these two respective contributions [22].

Difficulties in extracting η/s in heavy-ion collisions can be attributed mostly to the fact that it strongly depends on the specific choice of the initial conditions in the models used for comparison [4, 25, 26]. Viscous effects reduce the magnitude of the anisotropic flow. Furthermore, the magnitude of η/s used in hydrodynamic calculations should be considered as an average over the temperature evolution of the expanding fireball as it is known that η/s depends on temperature. In addition, part of the elliptic flow can also originate from the hadronic phase [27–29]. Therefore, both the temperature dependence of η/s and the relative contributions from the partonic and hadronic phases should be understood better to quantify the η/s of the QGP.

An important input to the hydrodynamic model simulations is the initial distribution of energy density in the transverse plane (the initial density profile), which is usually estimated from the probability distribution of nucleons in the incoming nuclei. This initial energy density profile can be quantified by calculating the distribution of the spatial eccentricities ε_n [20],

$$\varepsilon_n e^{in\Phi_n} = -\{r^n e^{in\phi}\}/\{r^n\}, \tag{2}$$

where the curly brackets denote the average over the transverse plane, i.e. $\{\cdots\} = \int dxdy\ e(x,y,\tau_0)\ (\cdots)$, r is the distance to the system's center of mass, $e(x,y,\tau_0)$ is the energy density at the initial time τ_0, and Φ_n is the participant plane angle (see Refs. [30, 31]). There is experimental and theoretical evidence [20, 21, 32] that the lower order harmonics, v_2 and v_3, to a good approximation, are linearly proportional to the deformations in the initial energy density in the transverse plane (e.g. $v_n \propto \varepsilon_n$ for $n = 2$ or 3). Higher order ($n > 3$) flow harmonics can arise from initial anisotropies in the same harmonic [20, 30, 33, 34] (linear response) or can be induced by lower order harmonics [35, 36] (nonlinear response). For instance, v_4 can develop both as a linear response to ε_4 and/or as a nonlinear response to ε_2^2. Therefore, the higher harmonics ($n > 3$) can be understood as superpositions of linear and nonlinear responses, through which they are correlated with lower order harmonics [33, 34, 36, 37]. When the order of the harmonic is large, the nonlinear response contribution in viscous hydrodynamics is dominant and increases in more peripheral collisions [36, 37]. The magnitudes of the viscous corrections as a function of p_{T} for v_4 and v_5 are sensitive to the ansatz used for the viscous distribution function, a correction for the equilibrium distribution at hadronic freeze-out [37, 38]. Hence, studies of the correlations between higher order ($n > 3$) and lower order (v_2 or v_3) harmonics and their p_{T} dependence can help to understand the viscous correction to the momentum distribution at hadronic freeze-out which is among the least understood parts of hydrodynamic calculations [31, 37, 39, 40].

The first results for new multiparticle observables which quantify the relationship between event-by-event fluctuations of two different flow harmonics, the *Symmetric Cumulants* (SC), were recently reported by the ALICE Collaboration [41]. The new observables are particularly robust against few-particle nonflow correlations and they provide independent, complementary information to recently analyzed symmetry plane correlators [23]. It was demonstrated that they are sensitive to the temperature dependence of η/s of the expanding medium and therefore simultaneous descriptions of correlations between different order harmonics would constrain both the initial conditions and the medium properties [41, 42]. In this article, we have extended the analysis of SC observables to higher order harmonics (up to 5$^{\text{th}}$ order) as well as to the measurement of the p_{T} dependence of correlations for the lower order harmonics (v_3-v_2 and v_4-v_2). We also present a systematic comparison to hydrodynamic and AMPT model calculations. In Sec. 2 we summarize our findings from the previous work [41] and present the analysis methods. The experimental setup and measurements are described in Sec. 3 and the sources of systematic uncertainties are explained in Sec. 4. The results of the measurements are presented in Sec. 5. In Sec. 6 we present comparisons to model calculations. Various models used in this article are described in Sec. 6. Finally, Sec. 7 summarizes our new results.

2 Experimental Observables

Existing measurements provide an estimate of the average value of η/s of the QGP, both at RHIC and LHC energies. What remains uncertain is how the η/s of the QGP depends on temperature (T). The temperature dependence of η/s of the QGP was discussed in [13]. The effects on hadron spectra and elliptic flow were studied in [43] for different parameterizations of $\eta/s(T)$. A more systematic study with event-by-event EKRT+viscous hydrodynamic calculations was recently initiated in [31], where the first (and only rather qualitative) possibilities were investigated (see Fig. 1 therein). The emerging picture is that the study of individual flow harmonics v_n alone is unlikely to reveal the details of the temperature dependence of η/s. It was already demonstrated in [31] that different $\eta/s(T)$ parameterizations can lead to the same centrality dependence of individual flow harmonics. In Ref. [22] new flow observables were introduced which quantify the degree of correlation between amplitudes of two different harmonics v_m

and v_n. These new observables have the potential to discriminate between the contributions to anisotropic flow development from initial conditions and from the transport properties of the QGP [22]. Therefore their measurement would provide experimental constraints on theoretical predictions for the individual stages of the heavy-ion system evolution independently. In addition, it turned out that correlations of different flow harmonics are sensitive to the temperature dependence of η/s [41], to which individual flow harmonics are weakly sensitive [31].

For reasons discussed in [41, 44], the correlations between different flow harmonics cannot be studied experimentally with the set of observables introduced in [22]. Based on [44], new flow observables obtained from multiparticle correlations, *Symmetric Cumulants* (SC), were introduced.

The SC observables are defined as:

$$\begin{aligned}\langle\langle\cos(m\varphi_1+n\varphi_2-m\varphi_3-n\varphi_4)\rangle\rangle_c &= \langle\langle\cos(m\varphi_1+n\varphi_2-m\varphi_3-n\varphi_4)\rangle\rangle \\ &\quad -\langle\langle\cos[m(\varphi_1-\varphi_2)]\rangle\rangle\langle\langle\cos[n(\varphi_1-\varphi_2)]\rangle\rangle \\ &= \left\langle v_m^2 v_n^2\right\rangle - \left\langle v_m^2\right\rangle\left\langle v_n^2\right\rangle ,\end{aligned} \tag{3}$$

with the condition $m \neq n$ for two positive integers m and n (for details see Sec. IV C in [44]). In this article SC(m,n) normalized by the product $\left\langle v_m^2\right\rangle\left\langle v_n^2\right\rangle$ [41, 45] is denoted by NSC(m,n):

$$\mathrm{NSC}(m,n) \equiv \frac{\mathrm{SC}(m,n)}{\langle v_m^2\rangle\langle v_n^2\rangle} . \tag{4}$$

Normalized symmetric cumulants reflect only the strength of the correlation between v_m and v_n, while $\mathrm{SC}(m,n)$ has contributions from both the correlations between the two different flow harmonics and the individual harmonics. In Eq. (4) the products in the denominator are obtained from two-particle correlations using a pseudorapidity gap of $|\Delta\eta| > 1.0$ which suppresses biases from few-particle nonflow correlations. For the two two-particle correlations which appear in the definition of $\mathrm{SC}(m,n)$ in Eq. (3) the pseudorapidity gap is not needed, since nonflow is suppressed by construction in this observable. This was verified by HIJING model simulations in [41].

The ALICE measurements [41] have revealed that fluctuations of v_2 and v_3 are anti-correlated, while fluctuations of v_2 and v_4 are correlated for all centralities [41]. It was found that the details of the centrality dependence differ in the fluctuation-dominated (most central) and the geometry-dominated (mid-central) regimes [41]. The observed centrality dependence of SC(4,2) cannot be captured by models with constant η/s, indicating that the temperature dependence of η/s plays an important role. These results were also used to discriminate between different parameterizations of initial conditions. It was demonstrated that in the fluctuation-dominated regime (central collisions), MC-Glauber initial conditions with binary collision weights are favored over wounded nucleon weights [41]. The first theoretical studies of SC observables can be found in Refs. [42, 45–48].

3 Data Analysis

Data recorded by ALICE in Pb–Pb collisions at $\sqrt{s_{\mathrm{NN}}} = 2.76$ TeV during the 2010 heavy-ion run at the LHC is used for this analysis. Detailed descriptions of the ALICE detector can be found in [49–51]. The Time Projection Chamber (TPC) was used to reconstruct charged particle tracks and measure their momenta with full azimuthal coverage in the pseudorapidity range $|\eta| < 0.8$. Two scintillator arrays (V0A and V0C) which cover the pseudorapidity ranges $-3.7 < \eta < -1.7$ and $2.8 < \eta < 5.1$ were used for triggering and the determination of centrality [52]. The trigger conditions and the event selection criteria are identical to those described in [2, 52]. Approximately 10^7 minimum-bias Pb–Pb events with a reconstructed primary vertex within ± 10 cm from the nominal interaction point along the beam direction are selected. Only charged particles reconstructed in the TPC in $|\eta| < 0.8$ and $0.2 < p_{\mathrm{T}} < 5$ GeV/c

were included in the analysis. The charged track quality cuts described in [2] were applied to minimize contamination from secondary charged particles and fake tracks. The track reconstruction efficiency and contamination were estimated from HIJING Monte Carlo simulations [53] combined with a GEANT3 [54] detector model and were found to be independent of the collision centrality. The reconstruction efficiency increases from 70% to 80% for particles with $0.2 < p_{\mathrm{T}} < 1$ GeV/c and remains constant at $(80 \pm 5)\%$ for $p_{\mathrm{T}} > 1$ GeV/c. The estimated contamination by secondary charged particles from weak decays and photon conversions is less than 6% at $p_{\mathrm{T}} = 0.2$ GeV/c and falls below 1% for $p_{\mathrm{T}} > 1$ GeV/c. The p_{T} cut-off of 0.2 GeV/c reduces event-by-event biases due to small reconstruction efficiency at lower p_{T}, while the high p_{T} cut-off of 5 GeV/c reduces the effects of jets on the measured correlations. Reconstructed TPC tracks were required to have at least 70 space points (out of a maximum of 159). Only tracks with a transverse distance of closest approach to the primary vertex less than 3 mm, both in the longitudinal and transverse directions, are accepted. This reduces the contamination from secondary tracks produced in the detector material, particles from weak decays, etc. Tracks with kinks (i.e. tracks that appear to change direction due to multiple scattering or $K^{\pm}$ decays) were rejected.

4 Systematic Uncertainties

The systematic uncertainties are estimated by varying the event and track selection criteria. All systematic checks described here are performed independently. The $\mathrm{SC}(m,n)$ values resulting from each variation are compared to ones from the default event and track selection described in the previous section, and differences are taken as the systematic uncertainty due to each individual source. The contributions from different sources were added in quadrature to obtain the total systematic uncertainty.

The event centrality was determined by the V0 detectors [55] with better than 2% resolution for the whole centrality range analyzed. The systematic uncertainty from the centrality determination was evaluated by using the TPC and Silicon Pixel Detector (SPD) [56] detectors instead of the V0 detectors. The systematic uncertainty on the symmetric cumulants which arises from the centrality uncertainty is about 3% both for SC(5,2) and SC(4,3), and 8% for SC(5,3). As described in Sec. 3, the reconstructed vertex position along the beam axis (z-vertex) is required to be located within 10 cm of the interaction point (IP) to ensure uniform detector acceptance for tracks within $|\eta| < 0.8$. The systematic uncertainty from the z-vertex cut was estimated by reducing the z-vertex range to 8 cm and was found to be less than 3%.

The analyzed events were recorded with two settings of the magnet field polarity and the resulting data sets have almost equal numbers of events. Events with both magnet field polarities were used in the default analysis, and the systematic uncertainties were evaluated from the variation between each of the two magnetic field settings. The uncertainty on the p_{T} dependent track reconstruction efficiency was also taken into account. Magnetic field polarity variation and reconstruction efficiency effects contribute less than 2% to the systematic uncertainty.

The systematic uncertainty due to the track reconstruction was estimated from comparisons between results for the so-called standalone TPC tracks with the same parameters as described in Sec. 3, and tracks from a combination of the TPC and the Inner Tracking System (ITS) detectors with tighter selection criteria. To avoid non-uniform azimuthal acceptance due to dead zones in the SPD, and to get the best transverse momentum resolution, a hybrid track selection utilizing SPD hits and/or ITS refit tracks combined with TPC information was used. Then each track reconstruction strategy was evaluated by varying the threshold on parameters used to select the tracks at the reconstruction level. A systematic difference of up to 12% was observed in $\mathrm{SC}(m,n)$ from the different track selections. In addition, we applied the like-sign technique to estimate nonflow contributions to $\mathrm{SC}(m,n)$. The difference between results obtained by selecting all charged particles and results obtained after either selecting only positively or only negatively charged particles was the largest contribution to the systematic uncertainty and is about 7% for SC(4,3) and 20% for SC(5,3).

Another large contribution to the systematic uncertainty originates from azimuthal non-uniformities in the reconstruction efficiency. In order to estimate its effects, we use the AMPT model (see Sec. 6) which has a uniform distribution in azimuthal angle. Detector inefficiencies were introduced to mimic the non-uniform azimuthal distribution in the data. For the observables SC(5,2), SC(5,3) and SC(4,3) the variation due to non-uniform acceptance is about 9%, 17% and 11%, respectively. Overall, the systematic uncertainties are larger for SC(5,3) and SC(5,2) than for the lower harmonics of SC(m,n). This is because v_n decreases with increasing n and becomes more sensitive to azimuthal modulation due to detector imperfections.

5 Results

The centrality dependence of the higher order harmonic correlations (SC(4,3), SC(5,2) and SC(5,3)) are presented in Fig. 1 and compared to the lower order harmonic correlations (SC(3,2) and SC(4,2)) which were measured in [41]. The correlation between v_3 and v_4 is negative, and similarly for v_3 and v_2, while the other correlations are all positive, which reveals that v_2 and v_5 as well as v_3 and v_5 are correlated like v_2 and v_4, while v_3 and v_4 are anti-correlated like v_3 and v_2.

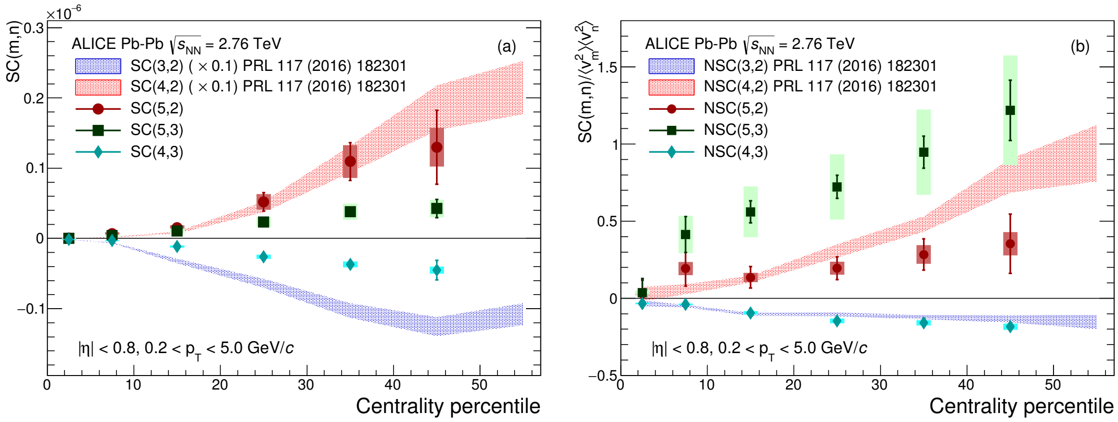

Fig. 1: The centrality dependence of SC(m,n) (a) and NSC(m,n) (b) with flow harmonics from 2$^{\mathrm{nd}}$ up to 5$^{\mathrm{th}}$ order in Pb–Pb collisions at $\sqrt{s_{\mathrm{NN}}} = 2.76$ TeV. The lower order harmonic correlations (SC(3,2), SC(4,2), NSC(3,2) and NSC(4,2)) are taken from [41] and shown as bands. Note that the systematic and statistical errors are combined in quadrature for these lower order harmonic correlations and SC(4,2) and SC(3,2) are scaled by a factor of 0.1. Systematic uncertainties are represented with boxes for higher order harmonic correlations.

The higher order flow harmonic correlations are much smaller compared to the lower order harmonic correlations. In particular SC(5,2) is 10 times smaller than SC(4,2) and SC(4,3) is about 20 times smaller than SC(3,2).

Unlike SC(m,n), the NSC(m,n) results with the higher order flow harmonics show almost the same order of the correlation strength as the lower order flow harmonic correlations (NSC(3,2) or NSC(4,2)). This demonstrates the advantage of using the normalized SC observables in which the correlation strength between flow harmonics is not hindered by the differences in magnitudes of different flow harmonics. The NSC(4,3) magnitude is comparable to NSC(3,2) and one finds that a hierarchy, NSC(5,3) $>$ NSC(4,2) $>$ NSC(5,2), holds for centrality ranges $>$ 20% within the errors as shown in Fig. 1(b). The SC(5,2) magnitude is larger than SC(5,3), but the normalized correlation between v_5 and v_3 is stronger than the normalized correlation between v_5 and v_2. These results indicate that the lower order harmonic correlations are larger than higher order harmonic correlations, not only because of the correlation strength itself but also because of the strength of the individual flow harmonics.

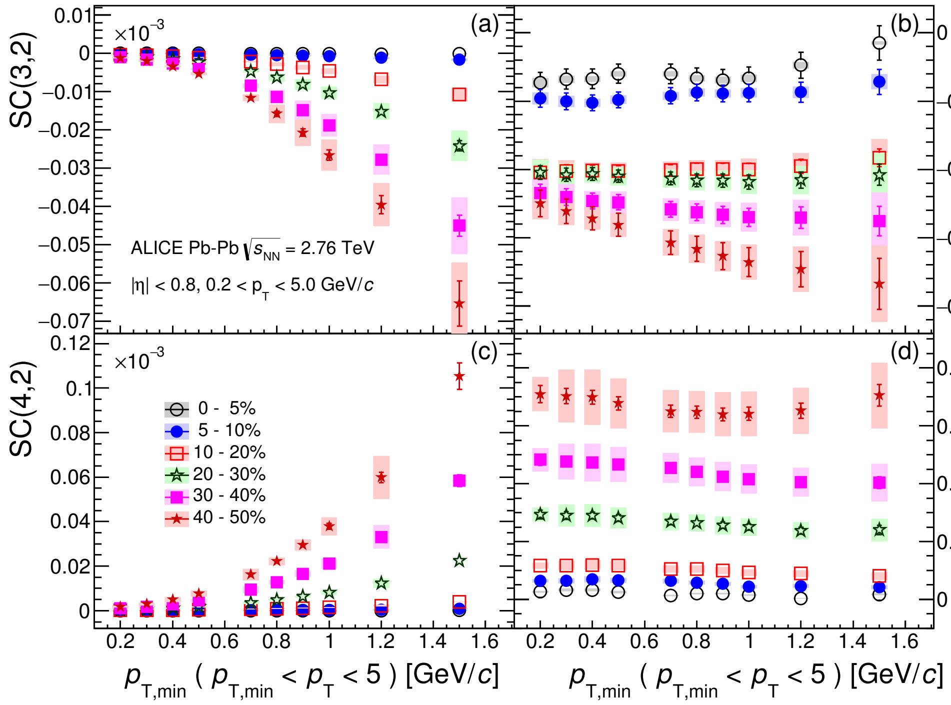

Fig. 2: SC(3,2) and SC(4,2) ((a) and (c)) as a function of minimum $p_{\rm T}$ cuts in Pb–Pb collisions at $\sqrt{s_{\rm NN}} = 2.76$ TeV are shown in the left panels. The normalized SC(3,2) and SC(4,2) ((b) and (d)) are shown in the right panels. Systematic uncertainties are represented with boxes.

It can be seen in Fig. 1(a) that the lower order harmonic correlations as well as SC(5,2) increase non-linearly towards peripheral collisions. In the case of SC(5,3) and SC(4,3), the centrality dependence is weaker than for the other harmonic correlations. The NSC(5,3) observable shows the strongest normalized correlation among all harmonics while NSC(5,2) shows the weakest centrality dependence. Both NSC(3,2) and NSC(4,3) are getting more anti-correlated toward peripheral collisions and have the similar magnitude.

To study the $p_{\rm T}$ dependence of SC(m,n), we show the results as a function of the low $p_{\rm T}$ cut-off ($p_{\rm T,min}$), instead of using independent $p_{\rm T}$ intervals; this avoids large statistical fluctuations in the results. Various minimum $p_{\rm T}$ cuts from 0.2 to 1.5 GeV/c are applied. The $p_{\rm T}$ dependent results for SC(3,2) and SC(4,2) as a function of minimum $p_{\rm T}$ cuts are shown in Figs. 2a and 2c. The strength of SC(m,n) becomes larger as $p_{\rm T,min}$ increases. The centrality dependence is stronger with higher $p_{\rm T,min}$ cuts, with SC(m,n) getting much larger as centrality or $p_{\rm T,min}$ increases. The NSC(3,2) and NSC(4,2) observables with different $p_{\rm T,min}$ are shown in Figs. 2b and 2d. The strong $p_{\rm T,min}$ dependence observed in SC(m,n) is not seen in NSC(m,n). This indicates that the $p_{\rm T}$ dependence of SC(m,n) is dominated by the $p_{\rm T}$ dependence of the individual flow harmonics $\langle v_n \rangle$. The $p_{\rm T,min}$ dependence of NSC(3,2) is not clearly seen and it is consistent with no $p_{\rm T,min}$ dependence within the statistical and systematic errors for the centrality range $< 30\%$, while showing a moderate increase of anti-correlation with increasing $p_{\rm T,min}$ for the $> 30\%$ centrality range. The NSC(4,2) observable shows a moderate decreasing trend as $p_{\rm T,min}$ increases. These observations are strikingly different from the $p_{\rm T}$ dependence of the individual flow harmonics, where the relative flow fluctuations $\sigma_{v_2}/\langle v_2 \rangle$ [57] are independent of transverse momentum up to $p_{\rm T} \sim 8$ GeV/c (see Fig. 3 in Ref. [58]).

As discussed in Sec. 2, the NSC(m,n) observables are normalized by the product $\langle v_m^2 \rangle \langle v_n^2 \rangle$. These products are obtained from two-particle correlations using a pseudorapidity gap of $|\Delta\eta| > 1.0$. We use

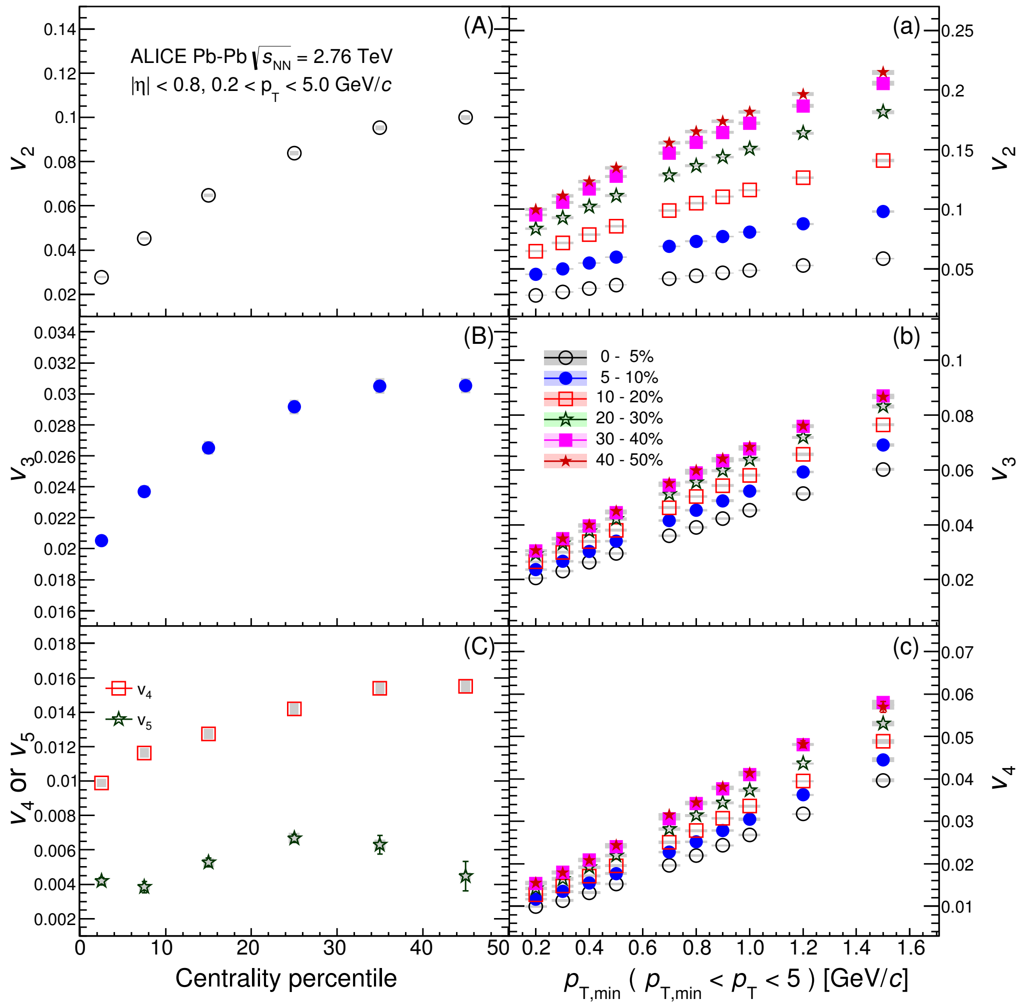

Fig. 3: The individual flow harmonics v_n ($n = 2$, 3, 4 and 5) in Pb–Pb collisions at $\sqrt{s_{NN}} = 2.76$ TeV are shown in the left panels ((A), (B) and (C)). The $p_{T,min}$ dependence of v_n ($n = 2$, 3 and 4) is shown in the right panels ((a), (b) and (c)). Note that v_5 is also shown in panel (C).

the notation v_n instead of $v_n\{2,|\Delta\eta|>1\}$ used in [3] and they are p_{T} integrated. The complete sets of the individual flow harmonics v_n used to calculate the NSC observables are shown in Fig. 3. The centrality dependence of v_n (n = 2, 3, 4 and 5) is shown in the left panels ((A), (B) and (C)) of Fig. 3. The v_n values ($n<5$) are equivalent to those in [3]. The 5$^{\mathrm{th}}$ order flow harmonic v_5 is shown in panel (C). The $p_{\mathrm{T,min}}$ dependence of v_n (n = 2, 3 and 4) is shown in the right panels ((a), (b) and (c)) of Fig. 3 in all centrality ranges relevant to the measured NSC(m,n) observables.

6 Model Comparisons

We have compared the centrality dependence of our observables with event-by-event EKRT+viscous hydrodynamic calculations [31], where the initial energy density profiles are calculated using a next-to-leading order perturbative-QCD+saturation model [59, 60]. The subsequent spacetime evolution is described by relativistic dissipative fluid dynamics with different parameterizations for the temperature dependence of the shear viscosity to entropy density ratio $\eta/s(T)$. This model gives a good description of the charged hadron multiplicity and the low p_{T} region of the charged hadron spectra at RHIC and the LHC (see Figs. 11-13 in [31]). Each of the $\eta/s(T)$ parameterizations is adjusted to reproduce the measured v_n from central to mid-peripheral collisions (see Fig. 15 in [31] and Appendix A).

The VISH2+1 [61, 62] event-by-event calculations for relativistic heavy-ion collisions are based on (2+1)-dimensional viscous hydrodynamics which describes both the QGP phase and the highly dissipative and even off-equilibrium late hadronic stage with fluid dynamics. With well-tuned transport coefficients and decoupling temperature, and given initial conditions discussed next, it can describe the p_{T} spectra and different flow harmonics at RHIC and the LHC [5, 61, 63, 64]. Three different initial conditions (MC-Glauber, MC-KLN and AMPT) along with different constant η/s values are used in the model [42]. Traditionally, the Glauber model constructs the initial entropy density with contributions from the wounded nucleon and binary collision density profiles [65], and the KLN model assumes that the initial entropy density is proportional to the initial gluon density calculated from the corresponding k_{T} factorization formula [66]. In MC-Glauber and MC-KLN [67–69], additional initial state fluctuations are introduced through position fluctuations of individual nucleons inside the colliding nuclei. For the AMPT initial conditions [64, 70, 71], the fluctuating energy density profiles are constructed from the energy decompositions of individual partons, which fluctuate in both momentum and spatial coordinates. Compared with the MC-Glauber and MC-KLN initial conditions, the additional Gaussian smearing in the AMPT initial conditions gives rise to non-vanishing initial local flow velocities [70]. The detailed quantitative comparisons of the measured v_n to the model calculations are provided in Appendix A.

Even though thermalization could be achieved in collisions of very large nuclei and/or at extremely high energy [75], the dense matter created in heavy-ion collisions may not reach full thermal or chemical equilibrium as a result of its finite volume and short lifetime. To address such non-equilibrium many-body dynamics, AMPT has been developed, which includes both initial partonic and final hadronic interactions and the transition between these two phases of matter. For the initial conditions, the AMPT model uses the spatial and momentum distributions of hard minijet partons and soft strings from the HIJING model [53, 76]. The AMPT model can be run in two main configurations, the default and the string melting model [1]. In the default version, partons are recombined with their parent strings when they stop interacting. The resulting strings are later converted into hadrons using the Lund string fragmentation model [77, 78]. In the string melting version, the initial strings are melted into partons whose interactions are described by the ZPC parton cascade model [79]. These partons are then combined into the final state hadrons via a quark coalescence model. In both configurations, the dynamics of the subsequent hadronic matter is described by a hadronic cascade based on A Relativistic Transport (ART) model [80] which also includes resonance decays. The third version used in this article is based on the string melting configu-

[1] The input parameters used in both configurations are: $\alpha_s = 0.33$, a partonic cross-section of 1.5 mb, while the Lund string fragmentation parameters were set to $\alpha = 0.5$ and $b = 0.9$ GeV^{-2}.

ration in which the hadronic rescattering phase is switched off to study its influence on the development of anisotropic flow. Even though the string melting version of AMPT [74, 81] reasonably reproduces particle yields, p_{T} spectra, and v_2 of low p_{T} pions and kaons in central and mid-central Au–Au collisions at $\sqrt{s_{\mathrm{NN}}} = 200$ GeV and Pb–Pb collisions at $\sqrt{s_{\mathrm{NN}}} = 2.76$ TeV [82], it was seen clearly in a recent study [83] that it fails to quantitatively reproduce the flow harmonics of identified hadrons (v_2, v_3, v_4 and v_5) at $\sqrt{s_{\mathrm{NN}}} = 2.76$ TeV. It turns out that the radial flow in AMPT is 25% lower than that measured at the LHC, which is responsible for this quantitative disagreement [83]. The details of the AMPT configurations used in this article and the comparisons of p_{T}-differential v_n for pions, kaons and protons to the data can be found in [83]. The quantitative comparisons of the measured v_n to various AMPT configurations are provided in Appendix A.

6.1 Centrality Dependence of SC(m,n) and NSC(m,n)

Three different models are compared with the experimental results presented in Sec. 5. We compare to event-by-event EKRT+viscous hydrodynamic predictions with various parameterizations of the temperature dependence of $\eta/s(T)$; these were shown in Fig. 2 of Ref. [41]. In this previous work it was demonstrated that NSC(3,2) is sensitive mainly to the initial conditions, while NSC(4,2) is sensitive to both the initial conditions and the system properties, which is consistent with the predictions from [22]. However, the sign of NSC(3,2) is negative in the data in 0–10% central collisions while it is positive in the models where the anisotropies originate mainly from fluctuations. This observation helps us to better understand the fluctuations in initial energy density. The NSC(4,2) observable shows better sensitivity for different $\eta/s(T)$ parameterizations but the model cannot describe either the centrality dependence or the absolute values. This observed discrepancy between data and theoretical predictions indicates that the current understanding of initial conditions in models of heavy-ion collisions needs to be revisited to further constrain $\eta/s(T)$. The measurement of SC(m,n) and NSC(m,n) can provide new constraints for the detailed modeling of fluctuating initial conditions.

While we discussed the comparison to these hydrodynamic model calculations with various temperature dependent η/s parameterizations, only two calculations with the parameters which describe the lower order harmonic correlations best are compared to the results in Fig. 4. As can be seen in Fig. 1 from Ref. [31], for the "param1" parameterization the phase transition from the hadronic to the QGP phase occurs at the lowest temperature, around 150 MeV. This parameterization is also characterized by a moderate slope in $\eta/s(T)$ which decreases (increases) in the hadronic (QGP) phase. The model calculations in which the temperature of the phase transition is larger than for "param1" can be ruled out by the previous measurements [41]. As shown in Fig. 4, the correlations between v_5 and v_2 are well described for all available centralities and similarly for the correlations between v_5 and v_3 within the errors. In the case of v_4 and v_3, the same models underestimate the anti-correlation in the data significantly in mid-central collisions and it fails similarly for the anti-correlation between v_3 and v_2. Most notably, this measurement is so far the most dramatic example of the failure of constant η/s to describe the data.

The comparison to the VISH2+1 calculation [42] is shown in Fig. 5. All calculations with large η/s regardless of the initial conditions ($\eta/s = 0.2$ for MC-KLN and MC-Glauber initial conditions and $\eta/s = 0.16$ for AMPT initial conditions) fail to capture the centrality dependence of the SC(m,n) observables of all orders, shown in the left panels in Fig. 5. Among the calculations with small η/s ($\eta/s = 0.08$), the one with the AMPT initial conditions describes the data better than the ones with other initial conditions for all SC(m,n) observables measured, but it cannot describe the data quantitively for most of the centrality ranges. Similar to the event-by-event EKRT+viscous hydrodynamic calculations [31], the sign of the normalized NSC(3,2) in the model calculations in Fig. 5 is opposite to that in data in 5–10% central collisions. NSC(3,2) and NSC(4,3) are not very sensitive to the initial conditions or η/s parameterization used in the model, and are not described quantitatively.

However, NSC(4,2) is sensitive both to the initial conditions and the η/s parameterizations used in the

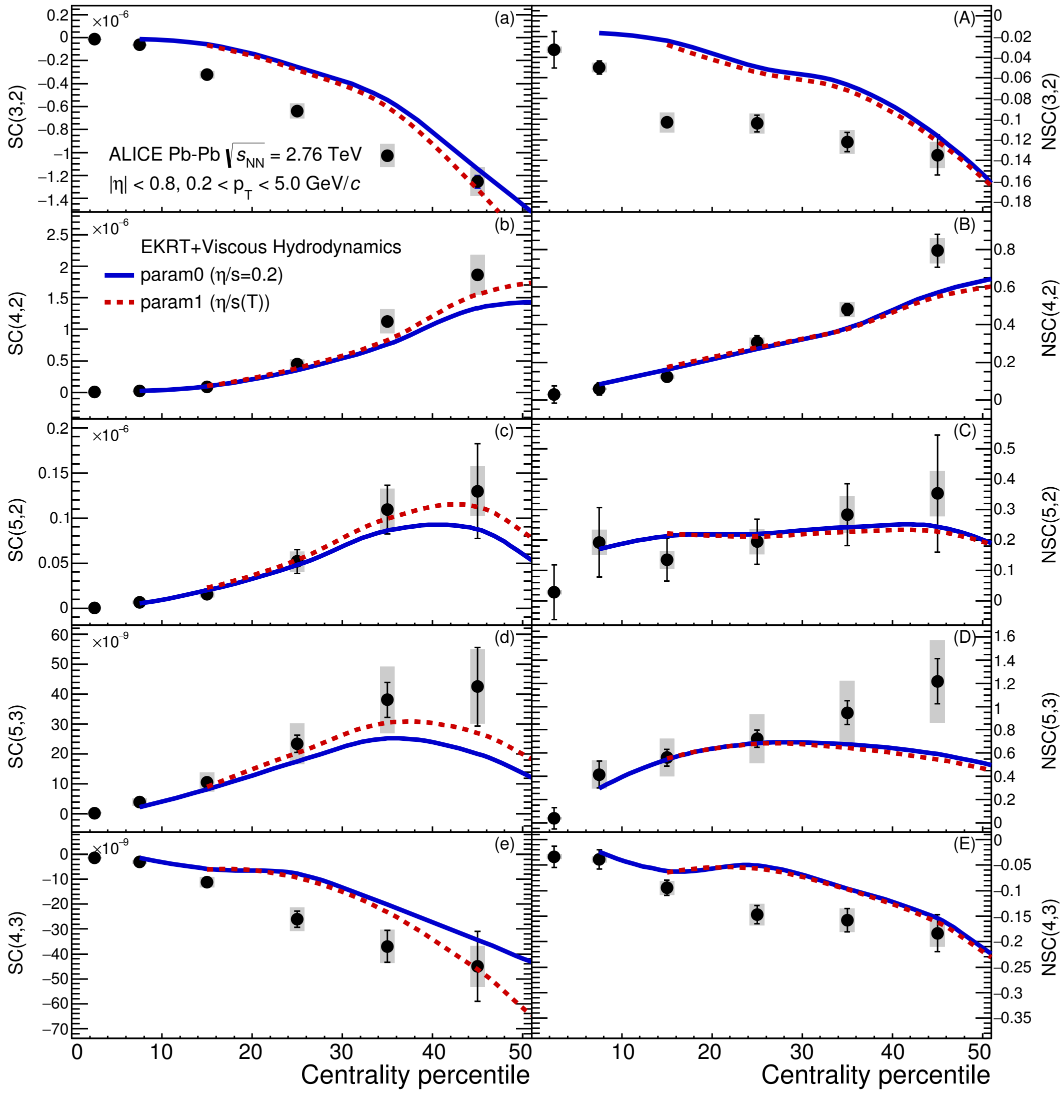

Fig. 4: The centrality dependence of SC(m,n) and NSC(m,n) in Pb–Pb collisions at $\sqrt{s_{NN}} = 2.76$ TeV are compared to the event-by-event EKRT+viscous hydrodynamic calculations [31]. The lines are hydrodynamic predictions with two different $\eta/s(T)$ parameterizations, labeled in the same way as in [31]. Left (right) panels show SC(m,n) (NSC(m,n)).

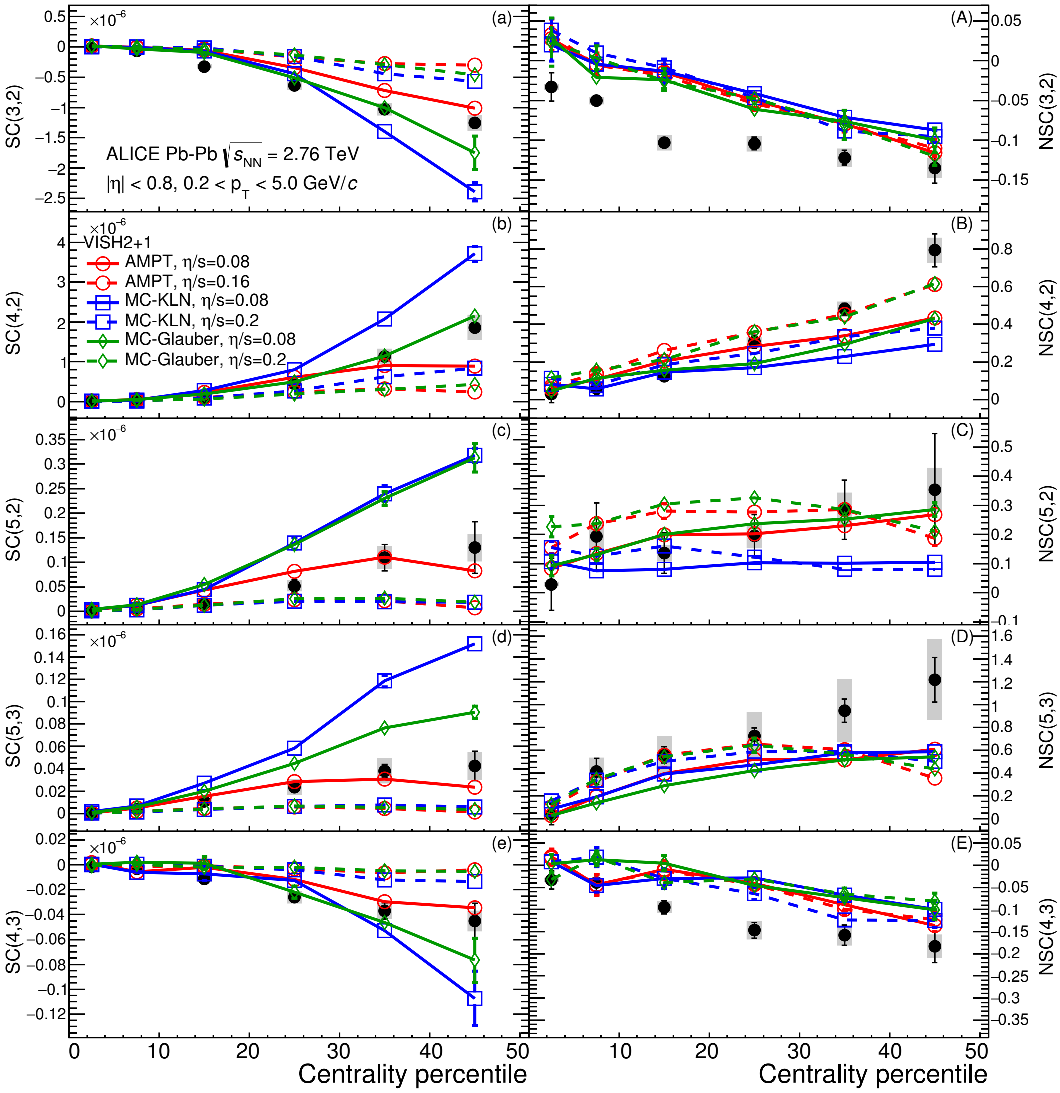

Fig. 5: The centrality dependence of SC(m,n) and NSC(m,n) in Pb–Pb collisions at $\sqrt{s_{NN}} = 2.76$ TeV are compared to various VISH2+1 calculations [42]. Three initial conditions from AMPT, MC-KLN and MC-Glauber are drawn as different colors and markers. The η/s parameters are shown as different line styles, the small shear viscosity ($\eta/s = 0.08$) are shown as solid lines, and large shear viscosities ($\eta/s = 0.2$ for MC-KLN and MC-Glauber, 0.16 for AMPT) are drawn as dashed lines. Left (right) panels show SC(m,n) (NSC(m,n)).

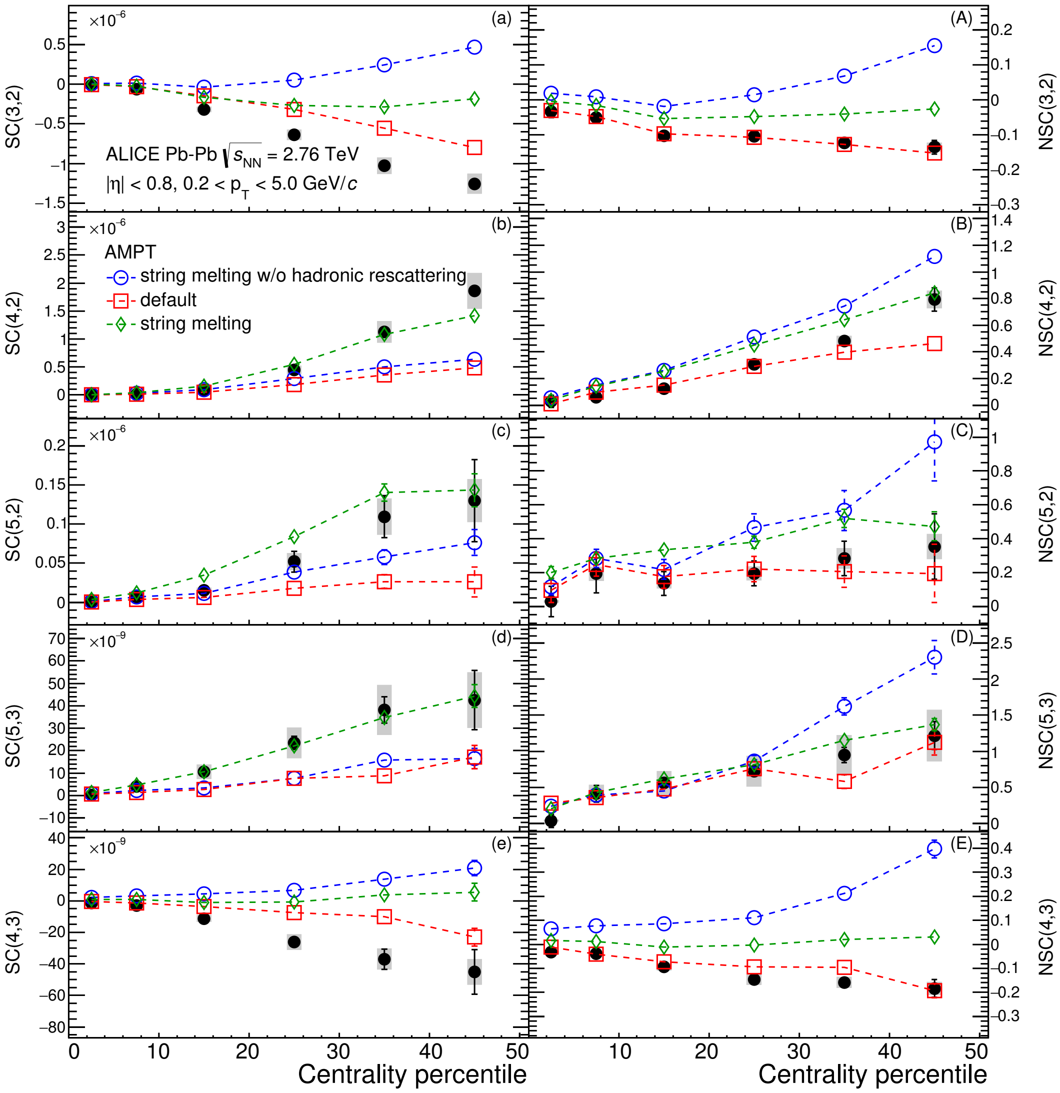

Fig. 6: The centrality dependence of SC(m,n) and NSC(m,n) in Pb–Pb collisions at $\sqrt{s_{\rm NN}} = 2.76$ TeV are compared to various AMPT models. Left (right) panels show SC(m,n) (NSC(m,n)).

models. Even though NSC(4,2) favors both AMPT initial conditions with $\eta/s = 0.08$ and MC-Glauber initial conditions with $\eta/s = 0.20$, SC(4,2) can only be described by models with smaller η/s. Hence the calculation with large $\eta/s = 0.20$ is ruled out. We conclude that η/s should be small and that AMPT initial conditions are favored by the data. The NSC(5,2) and NSC(5,3) observables are quite sensitive to both the initial conditions and the η/s parameterizations. Similar to the hydrodynamic calculations mentioned above [31], the sign of NSC(4,3) in these models is opposite to its sign in the data in 0–10% central collisions. The SC(4,3) results are clearly favored by smaller η/s values but NSC(4,3) cannot be described by these models quantitively.

The SC(m,n) and NSC(m,n) observables calculated from AMPT simulations are compared with data in Fig. 6. For SC(3,2), the calculation with the default AMPT settings is closest to the data, but none of the AMPT configurations can describe the data fully. The same default calculation can describe the sign and magnitude of NSC(3,2) while the hydrodynamic calculations fail to describe either of them in the most central collisions. The third version based on the string melting configuration without the hadronic rescattering phase is also shown. The hadronic rescattering stage makes both SC(3,2) and NSC(3,2) stronger in the string melting AMPT model but not enough to describe the data. Further investigations proved why the default AMPT model can describe NSC(3,2) fairly well but underestimates SC(3,2). By taking the differences in the individual flow harmonics (v_2 and v_3) between the model and data into account, it was possible to recover the difference in SC(3,2) between the data and the model. The discrepancy in SC(3,2) can be explained by the overestimated individual v_n values as reported in [83] in all centrality ranges.

In the case of SC(4,2), the string melting AMPT model can describe the data fairly well while the default model underestimates it. The NSC(4,2) observable is slightly overestimated by the string melting setting which can describe SC(4,2) but the default AMPT configuration can describe the data better. The influence of the hadronic rescattering phase on NSC(4,2) is opposite to other observables (SC(3,2), NSC(3,2) and SC(4,2)). The hadronic rescattering makes NSC(4,2) slightly smaller. It should be noted that the agreement with SC(m,n) should not be overemphasized since there are discrepancies in the individual v_n between the AMPT models and the data as was demonstrated for SC(3,2). Hence the simultaneous description of SC(m,n) and NSC(m,n) should give better constraints on the parameters in AMPT models. The string melting AMPT model describes SC(5,3) and NSC(5,3) well. However, the same setting overestimates SC(5,2) and NSC(5,2). The default AMPT model can describe NSC(5,3) and NSC(5,2) fairly well as in the case of NSC(3,2) and NSC(4,2). In the case of SC(4,3), neither of the settings can describe the data but the default AMPT model comes the closest to the data. The NSC(4,3) observable is well described by the default AMPT model but cannot be reproduced by the string melting AMPT model. In summary, the default AMPT model describes well the normalized symmetric cumulants (NSC(m,n)) from lower to higher order harmonic correlations while the string melting AMPT model overestimates NSC(3,2) and NSC(5,2) and predicts a very weak correlation both for NSC(3,2) and NSC(4,3).

As discussed in Sec. 5, a hierarchy NSC(5,3) $>$ NSC(4,2) $>$ NSC(5,2) holds for centrality ranges $>$ 20% within the errors. Except for the 0–10% centrality range, we found that the same hierarchy also holds in the hydrodynamic calculations and the AMPT models explored in this article. While NSC(5,2) is smaller than NSC(5,3), SC(5,2) is larger than SC(5,3). The observed reversal of the hierarchy, SC(5,2) $>$ SC(5,3), can be explained by the magnitudes of the individual flow harmonics ($v_2 > v_3$). This can be attributed to the fact that flow fluctuations are stronger for v_3 than v_2 [84]. This was claimed in Ref. [42] and also seen in Ref. [85] based on an AMPT model. NSC(m,n) correlators increase with larger η/s in hydrodynamic calculations in the 0–30% centrality range in the same way as the event plane correlations [86, 87]. In semi-peripheral collisions ($>$ 40%), the opposite trend is observed.

We list here the important findings from the model comparisons to the centrality dependence of SC(m,n) and NSC(m,n):

(i) The NSC(3,2) observable is sensitive mainly to the initial conditions, while the other observables are sensitive to both the initial conditions and the temperature dependence of η/s.

(ii) The correlation strength between v_3 and v_2 and between v_4 and v_3 (SC(3,2), SC(4,2), NSC(3,2) and NSC(4,3)) is significantly underestimated in hydrodynamic model calculations in mid-central collisions.

(iii) The sign of NSC(3,2) in 0–10% central collisions was found to be different in the data and the hydrodynamic model calculations while the default AMPT model can reproduce the sign.

(iv) All the VISH2+1 model calculations with large η/s fail to capture the centrality dependence of the correlations regardless of the initial conditions.

(v) Among the VISH2+1 model calculations with small η/s ($\eta/s = 0.08$), the one with the AMPT initial conditions captures the data qualitatively, but not quantitively for most of the centrality ranges.

(vi) The default AMPT model can describe the normalized symmetric cumulants (NSC(m,n)) quantitively for most centralities while the string melting AMPT model fails to describe them.

(vii) A hierarchy NSC(5,3) $>$ NSC(4,2) $>$ NSC(5,2) holds for centrality ranges $>$ 20% within the errors. This hierarchy is reproduced well both by hydrodynamic and AMPT model calculations.

6.2 Transverse Momentum Dependence of Correlations between v_2, v_3 and v_4

It can be seen in Fig. 2 that for NSC(3,2) there is no $p_{\mathrm{T,min}}$ dependence in the centrality range $<$ 30%, and a moderate decreasing trend with increasing $p_{\mathrm{T,min}}$ is observed in the $>$ 30% centrality range. NSC(4,2) shows a moderate decreasing trend as $p_{\mathrm{T,min}}$ or centrality increases.

The NSC(3,2) and NSC(4,2) observables as a function of $p_{\mathrm{T,min}}$ are compared to the AMPT simulations in Fig. 7 and Fig. 8, respectively. The observed p_{T} dependence for NSC(3,2) in mid-central collisions is also seen in AMPT simulations for higher minimum p_{T} cuts. With the exception of the default configuration, the other AMPT settings predict a very strong p_{T} dependence above 1 GeV/c and cannot describe the magnitudes of both NSC(3,2) and NSC(4,2) simultaneously. In the case of NSC(3,2), the default AMPT model describes the magnitude and p_{T} dependence well in all collision centralities except for 40–50% where the model underestimates the data and shows a stronger p_{T} dependence than the data. As for NSC(4,2), the same model which describes NSC(3,2) can also reproduce the data well except for the 10–20% and 40–50% centralities. When the string melting AMPT model is compared to the same model with the hadronic rescattering off, it is observed that the very strong p_{T} dependence as well as the correlation strength are weakened by the hadronic rescattering. Consequently, the observed weak p_{T} dependence may be due to hadronic rescattering. To clarify, the relative contributions to the final state particle distributions from partonic and hadronic stages need further study.

The event-by-event EKRT+viscous hydrodynamic calculations are also compared to the data in Fig. 7 and Fig. 8. In the case of NSC(3,2), the hydrodynamic calculations underestimate the magnitude of the data as discussed in Sec. 6.1 and show very weak p_{T} dependence for all centralities. The p_{T} dependence of NSC(3,2) is well captured by the model calculations in all collision centralities except for 40–50% where the data shows stronger p_{T} dependence than the models. The difference between the model calculations with the two different parameterizations of $\eta/s(T)$ is very small. As for NSC(4,2), the model calculations overestimate the magnitude of the data in the 5–20% centralities and underestimate it in the centrality range $>$ 20%. However, the p_{T} dependence is well described by the model calculations in all centrality ranges, while the difference of the model results for the two parameterizations in most centralities is rather small.

This observed moderate p_{T} dependence in mid-central collisions both for NSC(3,2) and NSC(4,2) might be an indication of possible viscous corrections to the equilibrium distribution at hadronic freeze-out, as predicted in [22]. The comparisons to hydrodynamic models can further help to understand the viscous corrections to the momentum distributions at hadronic freeze-out [31, 37–40].

7 Summary

In this article, we report the centrality dependence of correlations between the higher order harmonics (v_4, v_5) and the lower order harmonics (v_2, v_3) as well as the transverse momentum dependence of the correlations between v_3 and v_2 and between v_4 and v_2. The results are obtained with Symmetric 2-harmonic 4-particle Cumulants (SC). It was demonstrated earlier in [41] that this method is insensitive to nonflow effects and independent of symmetry plane correlations.

We have found that fluctuations of SC(3,2) and SC(4,3) are anti-correlated in all centralities while fluctuations of SC(4,2), SC(5,2) and SC(5,3) are correlated for all centralities. These measurements were

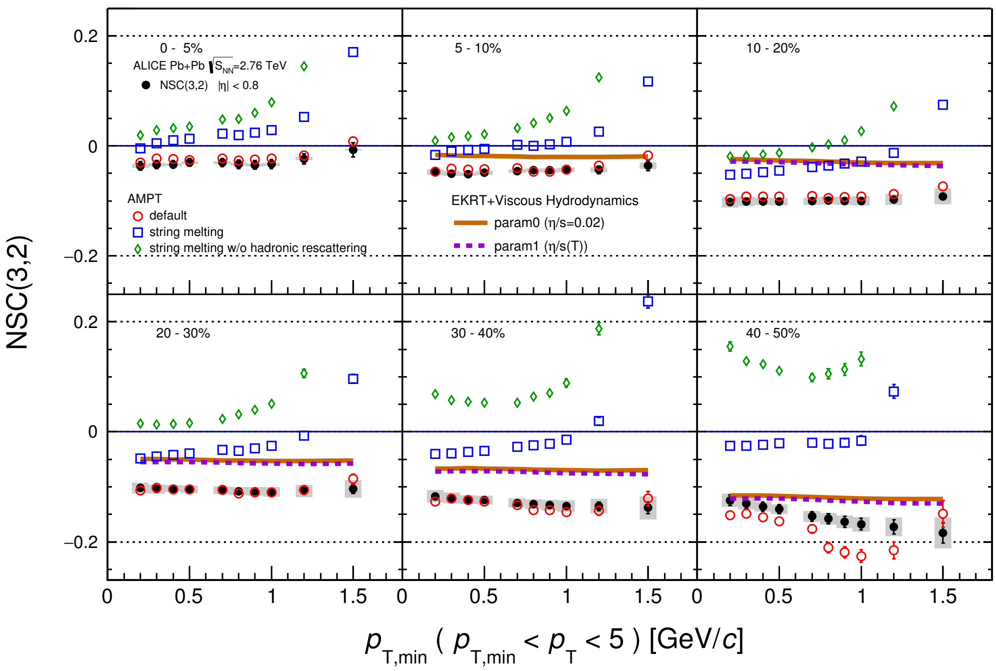

Fig. 7: NSC(3,2) as a function of the minimum p_{T} cut in Pb–Pb collisions at $\sqrt{s_{\mathrm{NN}}} = 2.76$ TeV is compared to various AMPT configurations and event-by-event EKRT+viscous hydrodynamic calculations [31].

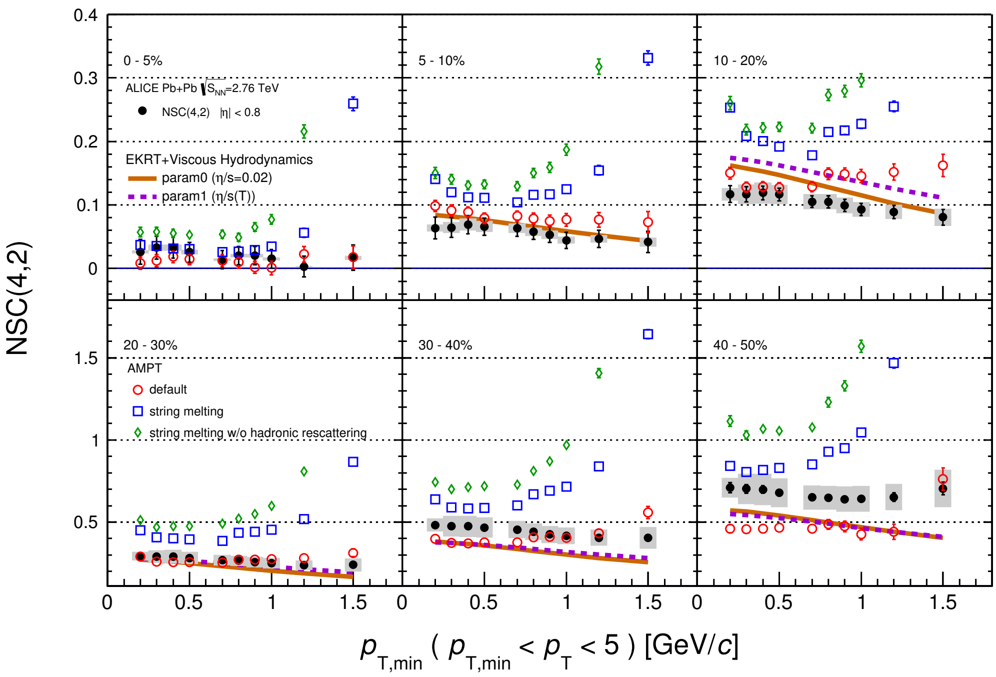

Fig. 8: NSC(4,2) as a function of the minimum p_{T} cut in Pb–Pb collisions at $\sqrt{s_{\mathrm{NN}}} = 2.76$ TeV is compared to various AMPT configurations and event-by-event EKRT+viscous hydrodynamic calculations [31].

compared to various hydrodynamic model calculations with different initial conditions as well as different parameterizations of the temperature dependence of η/s. It is found that the different order harmonic correlations have different sensitivities to the initial conditions and the system properties. Therefore they have discriminating power in separating the effects of η/s from the initial conditions on the final state particle anisotropies. The sign of SC(3,2) in 0–10% central collisions was found to be different between the data and hydrodynamic model calculations. In the most central collisions the anisotropies originate mainly from fluctuations, where the initial ellipsoidal geometry which dominates in mid-central collisions plays little role. This observation might help to understand the details of the fluctuations in the initial stage. The comparisons to VISH2+1 calculations show that all the models with large η/s, regardless of the initial conditions, fail to capture the centrality dependence of higher order correlations. Based on the tested model parameters, the data favors small η/s and the AMPT initial conditions.

A quite clear separation of the correlation strength for different initial conditions is observed for these higher order harmonic correlations compared to the lower order harmonic correlations. The default configuration of the AMPT model describes well the normalized symmetric cumulants (NSC(m,n)) for most centralities and for most combinations of harmonics which were considered. Finally, we have found that v_3 and v_2 as well as v_4 and v_2 correlations have moderate p_T dependence in mid-central collisions. This might be an indication of possible viscous corrections to the equilibrium distribution at hadronic freeze-out. Together with the measurements of individual harmonics these results can be used to further optimize model parameters and put better constraints on the initial conditions and the transport properties of nuclear matter in ultra-relativistic heavy-ion collisions.

Acknowledgements

References

[1] **STAR** Collaboration, K. H. Ackermann *et al.*, "Elliptic flow in Au + Au collisions at (S(NN))**(1/2) = 130 GeV," *Phys. Rev. Lett.* **86** (2001) 402–407, `arXiv:nucl-ex/0009011 [nucl-ex]`.

[2] **ALICE** Collaboration, K. Aamodt *et al.*, "Elliptic flow of charged particles in Pb-Pb collisions at 2.76 TeV," *Phys. Rev. Lett.* **105** (2010) 252302, `arXiv:1011.3914 [nucl-ex]`.

[3] **ALICE** Collaboration, J. Adam *et al.*, "Anisotropic flow of charged particles in Pb-Pb collisions at $\sqrt{s_{\rm NN}} = 5.02$ TeV," *Phys. Rev. Lett.* **116** no. 13, (2016) 132302, `arXiv:1602.01119 [nucl-ex]`.

[4] P. Romatschke and U. Romatschke, "Viscosity Information from Relativistic Nuclear Collisions: How Perfect is the Fluid Observed at RHIC?," *Phys. Rev. Lett.* **99** (2007) 172301, `arXiv:0706.1522 [nucl-th]`.

[5] C. Shen, U. Heinz, P. Huovinen, and H. Song, "Radial and elliptic flow in Pb+Pb collisions at the Large Hadron Collider from viscous hydrodynamic," *Phys. Rev.* **C84** (2011) 044903, `arXiv:1105.3226 [nucl-th]`.

[6] B. Schenke, S. Jeon, and C. Gale, "Elliptic and triangular flows in 3 + 1D viscous hydrodynamics with fluctuating initial conditions," *J. Phys.* **G38** (2011) 124169.

[7] P. Bozek and I. Wyskiel-Piekarska, "Particle spectra in Pb-Pb collisions at $\sqrt{S_N N} = 2.76 TeV$," *Phys. Rev.* **C85** (2012) 064915, `arXiv:1203.6513 [nucl-th]`.

[8] "Event-by-event anisotropic flow in heavy-ion collisions from combined Yang-Mills and viscous fluid dynamics," *Phys. Rev. Lett.* **110** no. 1, (2013) 012302, `arXiv:1209.6330 [nucl-th]`.

[9] T. Hirano, P. Huovinen, and Y. Nara, "Elliptic flow in Pb+Pb collisions at $\sqrt{s_{NN}} = 2.76$ TeV: hybrid model assessment of the first data," *Phys. Rev.* **C84** (2011) 011901, `arXiv:1012.3955 [nucl-th]`.

[10] P. Kovtun, D. T. Son, and A. O. Starinets, "Viscosity in strongly interacting quantum field theories from black hole physics," *Phys. Rev. Lett.* **94** (2005) 111601, `arXiv:hep-th/0405231 [hep-th]`.

[11] R. A. Lacey, N. N. Ajitanand, J. M. Alexander, P. Chung, W. G. Holzmann, M. Issah, A. Taranenko, P. Danielewicz, and H. Stoecker, "Has the QCD Critical Point been Signaled by Observations at RHIC?," *Phys. Rev. Lett.* **98** (2007) 092301, `arXiv:nucl-ex/0609025 [nucl-ex]`.

[12] P. Danielewicz and M. Gyulassy, "Dissipative phenomena in quark-gluon plasmas," *Phys. Rev. D* **31** (Jan, 1985) 53–62. `http://link.aps.org/doi/10.1103/PhysRevD.31.53`.

[13] L. P. Csernai, J. Kapusta, and L. D. McLerran, "On the Strongly-Interacting Low-Viscosity Matter Created in Relativistic Nuclear Collisions," *Phys. Rev. Lett.* **97** (2006) 152303, `arXiv:nucl-th/0604032 [nucl-th]`.

[14] J.-Y. Ollitrault, "Anisotropy as a signature of transverse collective flow," *Phys. Rev.* **D46** (1992) 229–245.

[15] S. Voloshin and Y. Zhang, "Flow study in relativistic nuclear collisions by Fourier expansion of Azimuthal particle distributions," *Z. Phys.* **C70** (1996) 665–672, `arXiv:hep-ph/9407282 [hep-ph]`.

[16] A. M. Poskanzer and S. A. Voloshin, "Methods for analyzing anisotropic flow in relativistic nuclear collisions," *Phys. Rev.* **C58** (1998) 1671–1678, `arXiv:nucl-ex/9805001 [nucl-ex]`.

[17] S. Floerchinger, U. A. Wiedemann, A. Beraudo, L. Del Zanna, G. Inghirami, and V. Rolando, "How (non-)linear is the hydrodynamics of heavy ion collisions?," *Phys. Lett.* **B735** (2014) 305–310, `arXiv:1312.5482 [hep-ph]`.

[18] M. Miller and R. Snellings, "Eccentricity fluctuations and its possible effect on elliptic flow measurements," `arXiv:nucl-ex/0312008 [nucl-ex]`.

[19] **PHOBOS** Collaboration, B. Alver *et al.*, "System size, energy, pseudorapidity, and centrality dependence of elliptic flow," *Phys. Rev. Lett.* **98** (2007) 242302, `arXiv:nucl-ex/0610037 [nucl-ex]`.

[20] B. Alver and G. Roland, "Collision geometry fluctuations and triangular flow in heavy-ion collisions," *Phys. Rev.* **C81** (2010) 054905, `arXiv:1003.0194 [nucl-th]`. [Erratum: Phys. Rev.C82,039903(2010)].

[21] **ALICE** Collaboration, K. Aamodt *et al.*, "Higher harmonic anisotropic flow measurements of charged particles in Pb-Pb collisions at $\sqrt{s_{NN}}$=2.76 TeV," *Phys. Rev. Lett.* **107** (2011) 032301, `arXiv:1105.3865 [nucl-ex]`.

[22] H. Niemi, G. S. Denicol, H. Holopainen, and P. Huovinen, "Event-by-event distributions of azimuthal asymmetries in ultrarelativistic heavy-ion collisions," *Phys. Rev.* **C87** no. 5, (2013) 054901, `arXiv:1212.1008 [nucl-th]`.

[23] **ATLAS** Collaboration, G. Aad *et al.*, "Measurement of event-plane correlations in $\sqrt{s_{NN}} = 2.76$ TeV lead-lead collisions with the ATLAS detector," *Phys. Rev.* **C90** no. 2, (2014) 024905, `arXiv:1403.0489 [hep-ex]`.

[24] B. H. Alver, C. Gombeaud, M. Luzum, and J.-Y. Ollitrault, “Triangular flow in hydrodynamics and transport theory,” *Phys. Rev.* **C82** (2010) 034913, `arXiv:1007.5469 [nucl-th]`.

[25] M. Luzum and J.-Y. Ollitrault, “Extracting the shear viscosity of the quark-gluon plasma from flow in ultra-central heavy-ion collisions,” *Nucl. Phys.* **A904-905** (2013) 377c–380c, `arXiv:1210.6010 [nucl-th]`.

[26] C. Shen, S. A. Bass, T. Hirano, P. Huovinen, Z. Qiu, H. Song, and U. Heinz, “The QGP shear viscosity: Elusive goal or just around the corner?,” *J. Phys.* **G38** (2011) 124045, `arXiv:1106.6350 [nucl-th]`.

[27] P. Bozek, “Flow and interferometry in 3+1 dimensional viscous hydrodynamics,” *Phys. Rev.* **C85** (2012) 034901, `arXiv:1110.6742 [nucl-th]`.

[28] J.-B. Rose, J.-F. Paquet, G. S. Denicol, M. Luzum, B. Schenke, S. Jeon, and C. Gale, “Extracting the bulk viscosity of the quark?gluon plasma,” *Nucl. Phys.* **A931** (2014) 926–930, `arXiv:1408.0024 [nucl-th]`.

[29] S. Ryu, J. F. Paquet, C. Shen, G. S. Denicol, B. Schenke, S. Jeon, and C. Gale, “Importance of the Bulk Viscosity of QCD in Ultrarelativistic Heavy-Ion Collisions,” *Phys. Rev. Lett.* **115** no. 13, (2015) 132301, `arXiv:1502.01675 [nucl-th]`.

[30] D. Teaney and L. Yan, “Triangularity and Dipole Asymmetry in Heavy Ion Collisions,” *Phys. Rev.* **C83** (2011) 064904, `arXiv:1010.1876 [nucl-th]`.

[31] H. Niemi, K. J. Eskola, and R. Paatelainen, “Event-by-event fluctuations in a perturbative QCD + saturation + hydrodynamics model: Determining QCD matter shear viscosity in ultrarelativistic heavy-ion collisions,” *Phys. Rev.* **C93** no. 2, (2016) 024907, `arXiv:1505.02677 [hep-ph]`.

[32] Z. Qiu and U. W. Heinz, “Event-by-event shape and flow fluctuations of relativistic heavy-ion collision fireballs,” *Phys. Rev.* **C84** (2011) 024911, `arXiv:1104.0650 [nucl-th]`.

[33] S. S. Gubser and A. Yarom, “Conformal hydrodynamics in Minkowski and de Sitter spacetimes,” *Nucl. Phys.* **B846** (2011) 469–511, `arXiv:1012.1314 [hep-th]`.

[34] Y. Hatta, J. Noronha, G. Torrieri, and B.-W. Xiao, “Flow harmonics within an analytically solvable viscous hydrodynamic model,” *Phys. Rev.* **D90** no. 7, (2014) 074026, `arXiv:1407.5952 [hep-ph]`.

[35] L. V. Bravina, B. H. Brusheim Johansson, G. K. Eyyubova, V. L. Korotkikh, I. P. Lokhtin, L. V. Malinina, S. V. Petrushanko, A. M. Snigirev, and E. E. Zabrodin, “Higher harmonics of azimuthal anisotropy in relativistic heavy ion collisions in HYDJET++ model,” *Eur. Phys. J.* **C74** no. 3, (2014) 2807, `arXiv:1311.7054 [nucl-th]`.

[36] L. V. Bravina, B. H. Brusheim Johansson, G. K. Eyyubova, V. L. Korotkikh, I. P. Lokhtin, L. V. Malinina, S. V. Petrushanko, A. M. Snigirev, and E. E. Zabrodin, “Hexagonal flow v6 as a superposition of elliptic v2 and triangular v3 flows,” *Phys. Rev.* **C89** no. 2, (2014) 024909, `arXiv:1311.0747 [hep-ph]`.

[37] D. Teaney and L. Yan, “Non linearities in the harmonic spectrum of heavy ion collisions with ideal and viscous hydrodynamics,” *Phys. Rev.* **C86** (2012) 044908, `arXiv:1206.1905 [nucl-th]`.

[38] M. Luzum and J.-Y. Ollitrault, “Constraining the viscous freeze-out distribution function with data obtained at the BNL Relativistic Heavy Ion Collider (RHIC),” *Phys. Rev.* **C82** (2010) 014906, `arXiv:1004.2023 [nucl-th]`.

[39] K. Dusling, G. D. Moore, and D. Teaney, "Radiative energy loss and v(2) spectra for viscous hydrodynamics," *Phys. Rev.* **C81** (2010) 034907, `arXiv:0909.0754 [nucl-th]`.

[40] D. Molnar and Z. Wolff, "Self-consistent conversion of a viscous fluid to particles," `arXiv:1404.7850 [nucl-th]`.

[41] **ALICE** Collaboration, J. Adam *et al.*, "Correlated event-by-event fluctuations of flow harmonics in Pb-Pb collisions at $\sqrt{s_{\rm NN}} = 2.76$ TeV," *Phys. Rev. Lett.* **117** (2016) 182301, `arXiv:1604.07663 [nucl-ex]`.

[42] X. Zhu, Y. Zhou, H. Xu, and H. Song, "Correlations of flow harmonics in 2.76A TeV Pb–Pb collisions," `arXiv:1608.05305 [nucl-th]`.

[43] H. Niemi, G. S. Denicol, P. Huovinen, E. Molnar, and D. H. Rischke, "Influence of the shear viscosity of the quark-gluon plasma on elliptic flow in ultrarelativistic heavy-ion collisions," *Phys. Rev. Lett.* **106** (2011) 212302, `arXiv:1101.2442 [nucl-th]`.

[44] A. Bilandzic, C. H. Christensen, K. Gulbrandsen, A. Hansen, and Y. Zhou, "Generic framework for anisotropic flow analyses with multiparticle azimuthal correlations," *Phys. Rev.* **C89** no. 6, (2014) 064904, `arXiv:1312.3572 [nucl-ex]`.

[45] G. Giacalone, L. Yan, J. Noronha-Hostler, and J.-Y. Ollitrault, "Symmetric cumulants and event-plane correlations in Pb + Pb collisions," *Phys. Rev.* **C94** no. 1, (2016) 014906, `arXiv:1605.08303 [nucl-th]`.

[46] J. Qian and U. Heinz, "Hydrodynamic flow amplitude correlations in event-by-event fluctuating heavy-ion collisions," *Phys. Rev.* **C94** no. 2, (2016) 024910, `arXiv:1607.01732 [nucl-th]`.

[47] F. G. Gardim, F. Grassi, M. Luzum, and J. Noronha-Hostler, "Hydrodynamic Predictions for Mixed Harmonic Correlations in 200 GeV Au+Au Collisions," `arXiv:1608.02982 [nucl-th]`.

[48] W. Ke, J. S. Moreland, J. E. Bernhard, and S. A. Bass, "Constraints on rapidity-dependent initial conditions from charged particle pseudorapidity densities and two-particle correlations," `arXiv:1610.08490 [nucl-th]`.

[49] **ALICE** Collaboration, K. Aamodt *et al.*, "The ALICE experiment at the CERN LHC," *JINST* **3** (2008) S08002.

[50] **ALICE** Collaboration, P. Cortese *et al.*, "ALICE: Physics performance report, volume I," *J. Phys.* **G30** (2004) 1517–1763.

[51] **ALICE** Collaboration, P. Cortese *et al.*, "ALICE: Physics performance report, volume II," *J. Phys.* **G32** (2006) 1295–2040.

[52] **ALICE** Collaboration, K. Aamodt *et al.*, "Centrality dependence of the charged-particle multiplicity density at mid-rapidity in Pb-Pb collisions at $\sqrt{s_{NN}} = 2.76$ TeV," *Phys. Rev. Lett.* **106** (2011) 032301, `arXiv:1012.1657 [nucl-ex]`.

[53] X.-N. Wang and M. Gyulassy, "HIJING: A Monte Carlo model for multiple jet production in p p, p A and A A collisions," *Phys. Rev.* **D44** (1991) 3501–3516.

[54] "GEANT Detector Description and Simulation Tool,".

[55] **ALICE** Collaboration, E. Abbas *et al.*, "Performance of the ALICE VZERO system," *JINST* **8** (2013) P10016, `arXiv:1306.3130 [nucl-ex]`.

[56] **ALICE** Collaboration, G. Dellacasa *et al.*, "ALICE technical design report of the inner tracking system (ITS),".

[57] S. A. Voloshin, A. M. Poskanzer, and R. Snellings, "Collective phenomena in non-central nuclear collisions," `arXiv:0809.2949 [nucl-ex]`.

[58] **ALICE** Collaboration, B. Abelev *et al.*, "Anisotropic flow of charged hadrons, pions and (anti-)protons measured at high transverse momentum in Pb-Pb collisions at $\sqrt{s_{NN}}$=2.76 TeV," *Phys. Lett.* **B719** (2013) 18–28, `arXiv:1205.5761 [nucl-ex]`.

[59] R. Paatelainen, K. J. Eskola, H. Holopainen, and K. Tuominen, "Multiplicities and p_T spectra in ultrarelativistic heavy ion collisions from a next-to-leading order improved perturbative QCD + saturation + hydrodynamics model," *Phys. Rev.* **C87** no. 4, (2013) 044904, `arXiv:1211.0461 [hep-ph]`.

[60] R. Paatelainen, K. J. Eskola, H. Niemi, and K. Tuominen, "Fluid dynamics with saturated minijet initial conditions in ultrarelativistic heavy-ion collisions," *Phys. Lett.* **B731** (2014) 126–130, `arXiv:1310.3105 [hep-ph]`.

[61] C. Shen, U. Heinz, P. Huovinen, and H. Song, "Systematic parameter study of hadron spectra and elliptic flow from viscous hydrodynamic simulations of Au+Au collisions at $\sqrt{s_{NN}} = 200$ GeV," *Phys. Rev.* **C82** (2010) 054904, `arXiv:1010.1856 [nucl-th]`.

[62] C. Shen, Z. Qiu, H. Song, J. Bernhard, S. Bass, and U. Heinz, "The iEBE-VISHNU code package for relativistic heavy-ion collisions," *Comput. Phys. Commun.* **199** (2016) 61–85, `arXiv:1409.8164 [nucl-th]`.

[63] Z. Qiu, C. Shen, and U. Heinz, "Hydrodynamic elliptic and triangular flow in Pb-Pb collisions at $\sqrt{s} = 2.76$ATeV," *Phys. Lett.* **B707** (2012) 151–155, `arXiv:1110.3033 [nucl-th]`.

[64] R. S. Bhalerao, A. Jaiswal, and S. Pal, "Collective flow in event-by-event partonic transport plus hydrodynamics hybrid approach," *Phys. Rev.* **C92** no. 1, (2015) 014903, `arXiv:1503.03862 [nucl-th]`.

[65] P. F. Kolb, J. Sollfrank, and U. W. Heinz, "Anisotropic transverse flow and the quark hadron phase transition," *Phys. Rev.* **C62** (2000) 054909, `arXiv:hep-ph/0006129 [hep-ph]`.

[66] D. Kharzeev and M. Nardi, "Hadron production in nuclear collisions at RHIC and high density QCD," *Phys. Lett.* **B507** (2001) 121–128, `arXiv:nucl-th/0012025 [nucl-th]`.

[67] M. L. Miller, K. Reygers, S. J. Sanders, and P. Steinberg, "Glauber modeling in high energy nuclear collisions," *Ann. Rev. Nucl. Part. Sci.* **57** (2007) 205–243, `arXiv:nucl-ex/0701025 [nucl-ex]`.

[68] H. J. Drescher and Y. Nara, "Effects of fluctuations on the initial eccentricity from the Color Glass Condensate in heavy ion collisions," *Phys. Rev.* **C75** (2007) 034905, `arXiv:nucl-th/0611017 [nucl-th]`.

[69] T. Hirano and Y. Nara, "Eccentricity fluctuation effects on elliptic flow in relativistic heavy ion collisions," *Phys. Rev.* **C79** (2009) 064904, `arXiv:0904.4080 [nucl-th]`.

[70] L. Pang, Q. Wang, and X.-N. Wang, "Effects of initial flow velocity fluctuation in event-by-event (3+1)D hydrodynamics," *Phys. Rev.* **C86** (2012) 024911, `arXiv:1205.5019 [nucl-th]`.

[71] H.-j. Xu, Z. Li, and H. Song, "High-order flow harmonics of identified hadrons in 2.76A TeV Pb + Pb collisions," *Phys. Rev.* **C93** no. 6, (2016) 064905, `arXiv:1602.02029 [nucl-th]`.

[72] B. Zhang, C. M. Ko, B.-A. Li, and Z.-w. Lin, "A multiphase transport model for nuclear collisions at RHIC," *Phys. Rev.* **C61** (2000) 067901, `arXiv:nucl-th/9907017 [nucl-th]`.

[73] Z.-w. Lin, S. Pal, C. M. Ko, B.-A. Li, and B. Zhang, "Charged particle rapidity distributions at relativistic energies," *Phys. Rev.* **C64** (2001) 011902, `arXiv:nucl-th/0011059 [nucl-th]`.

[74] Z.-W. Lin, C. M. Ko, B.-A. Li, B. Zhang, and S. Pal, "A Multi-phase transport model for relativistic heavy ion collisions," *Phys. Rev.* **C72** (2005) 064901, `arXiv:nucl-th/0411110 [nucl-th]`.

[75] A. Kurkela and Y. Zhu, "Isotropization and hydrodynamization in weakly coupled heavy-ion collisions," *Phys. Rev. Lett.* **115** no. 18, (2015) 182301, `arXiv:1506.06647 [hep-ph]`.

[76] M. Gyulassy and X.-N. Wang, "HIJING 1.0: A Monte Carlo program for parton and particle production in high-energy hadronic and nuclear collisions," *Comput. Phys. Commun.* **83** (1994) 307, `arXiv:nucl-th/9502021 [nucl-th]`.

[77] B. Andersson, G. Gustafson, and B. Nilsson-Almqvist, "A Model for Low p(t) Hadronic Reactions, with Generalizations to Hadron - Nucleus and Nucleus-Nucleus Collisions," *Nucl. Phys.* **B281** (1987) 289–309.

[78] B. Nilsson-Almqvist and E. Stenlund, "Interactions Between Hadrons and Nuclei: The Lund Monte Carlo, Fritiof Version 1.6," *Comput. Phys. Commun.* **43** (1987) 387.

[79] B. Zhang, "ZPC 1.0.1: A Parton cascade for ultrarelativistic heavy ion collisions," *Comput. Phys. Commun.* **109** (1998) 193–206, `arXiv:nucl-th/9709009 [nucl-th]`.

[80] B. Li, A. T. Sustich, B. Zhang, and C. M. Ko, "Studies of superdense hadronic matter in a relativistic transport model," *Int. J. Mod. Phys.* **E10** (2001) 267–352.

[81] Z.-w. Lin and C. M. Ko, "Partonic effects on the elliptic flow at RHIC," *Phys. Rev.* **C65** (2002) 034904, `arXiv:nucl-th/0108039 [nucl-th]`.

[82] Z.-W. Lin, "Evolution of transverse flow and effective temperatures in the parton phase from a multi-phase transport model," *Phys. Rev.* **C90** no. 1, (2014) 014904, `arXiv:1403.6321 [nucl-th]`.

[83] **ALICE** Collaboration, J. Adam *et al.*, "Higher harmonic flow coefficients of identified hadrons in Pb-Pb collisions at $\sqrt{s_{\rm NN}}$ = 2.76 TeV," *JHEP* **09** (2016) 164, `arXiv:1606.06057 [nucl-ex]`.

[84] **ATLAS** Collaboration, G. Aad *et al.*, "Measurement of the distributions of event-by-event flow harmonics in lead-lead collisions at = 2.76 TeV with the ATLAS detector at the LHC," *JHEP* **11** (2013) 183, `arXiv:1305.2942 [hep-ex]`.

[85] R. S. Bhalerao, J.-Y. Ollitrault, and S. Pal, "Characterizing flow fluctuations with moments," *Phys. Lett.* **B742** (2015) 94–98, `arXiv:1411.5160 [nucl-th]`.

[86] R. S. Bhalerao, J.-Y. Ollitrault, and S. Pal, "Event-plane correlators," *Phys. Rev.* **C88** (2013) 024909, `arXiv:1307.0980 [nucl-th]`.

[87] D. Teaney and L. Yan, "Event-plane correlations and hydrodynamic simulations of heavy ion collisions," *Phys. Rev.* **C90** no. 2, (2014) 024902, `arXiv:1312.3689 [nucl-th]`.

A Model Comparisons of the Individual Flow Harmonics v_n

As discussed in Sec. 2, NSC(m,n) is expected to be insensitive to the magnitudes of v_m and v_n but SC(m,n) has contributions from both the correlations between the two different flow harmonics and the individual harmonics v_n. Therefore it is important to check how well the theoretical models used in Sec. 6 describe the measured v_n data shown in Sec. 5. The comparisons are made only up to v_4 because model calculations are not available for v_5 at this moment.

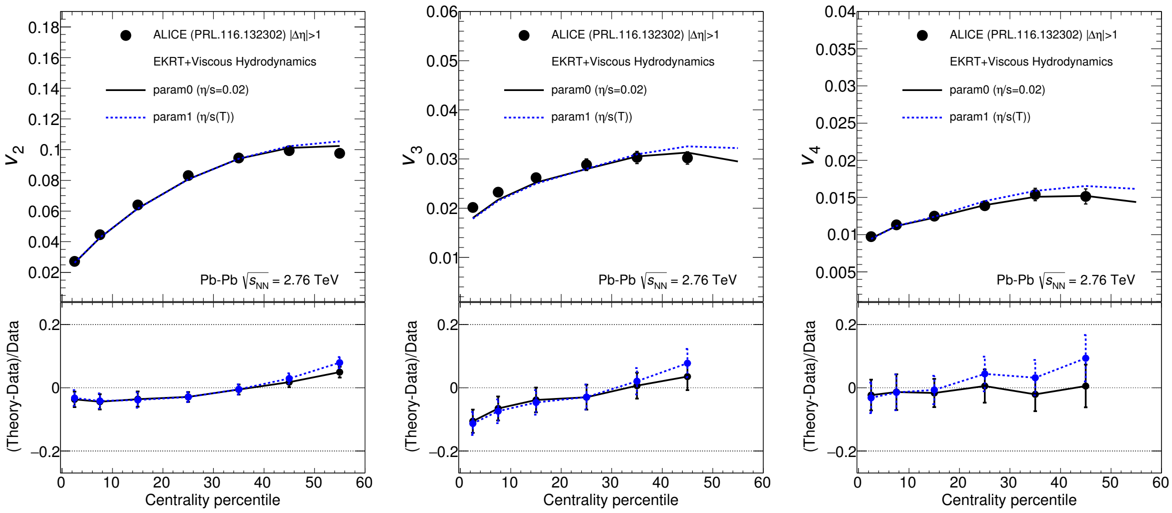

Fig. A.1: The individual flow harmonics v_n (n = 2, 3 and 4) in Pb–Pb collisions at $\sqrt{s_{\rm NN}}$ = 2.76 TeV [3] are compared to the event-by-event EKRT+viscous hydrodynamic calculations [31]. The lines are hydrodynamic predictions with two different $\eta/s(T)$ parameterizations, labeled in the same way as in [31].

The measured v_n (n = 2, 3 and 4) in Pb–Pb collisions at $\sqrt{s_{\rm NN}}$ = 2.76 TeV are compared to the event-by-event EKRT+viscous hydrodynamic calculations [31] in Fig. A.1. In these calculations the initial conditions and η/s parameterizations are chosen to reproduce the LHC v_n data. The calculations capture the centrality dependence of v_n in the central and midcentral collisions within 5% for v_2 and 10% for v_3 and v_4.

The VISH2+1 calculations with various initial conditions and η/s parameters are compared to the v_n data in Fig. A.2. Neither MC-Glauber nor MC-KLN initial conditions can simultaneously describe v_2, v_3 and v_4. In particular, for MC-Glauber initial conditions, VISH2+1 with $\eta/s = 0.08$ can describe well v_2 from central to midcentral collisions, but overestimates v_3 and v_4 for the same centrality ranges. For MC-KLN initial conditions, VISH2+1 with $\eta/s = 0.20$ reproduces v_2 but underestimates v_3 and v_4 for the presented centrality regions. The calculations with AMPT initial conditions improves the simultaneous descriptions of v_n (n = 2, 3 and 4). The overall difference to the data is quite large if all the model settings are considered, about 30% for v_n (n = 2 and 3) and 50% for v_4. The calculations with AMPT initial conditions reproduce the observed centrality dependence with an accuracy of 10-20%.

The AMPT calculations with various configurations are compared to the v_n data in Fig. A.3. The string melting version of AMPT [74, 81] reasonably reproduces v_n as shown in Fig. A.3 within 20% for v_2 and 10% for v_3 and v_4. The version based on the string melting configuration without the hadronic rescattering phase underestimates the data compared to the calculations with the string melting version of AMPT, which demonstrates that a large fraction of the flow is developed during the late hadronic rescattering stage in the string melting version of AMPT. The default version of AMPT underestimates v_n (n = 2, 3 and 4) by $\approx$ 20%. It should be noted that the default AMPT model can describe the

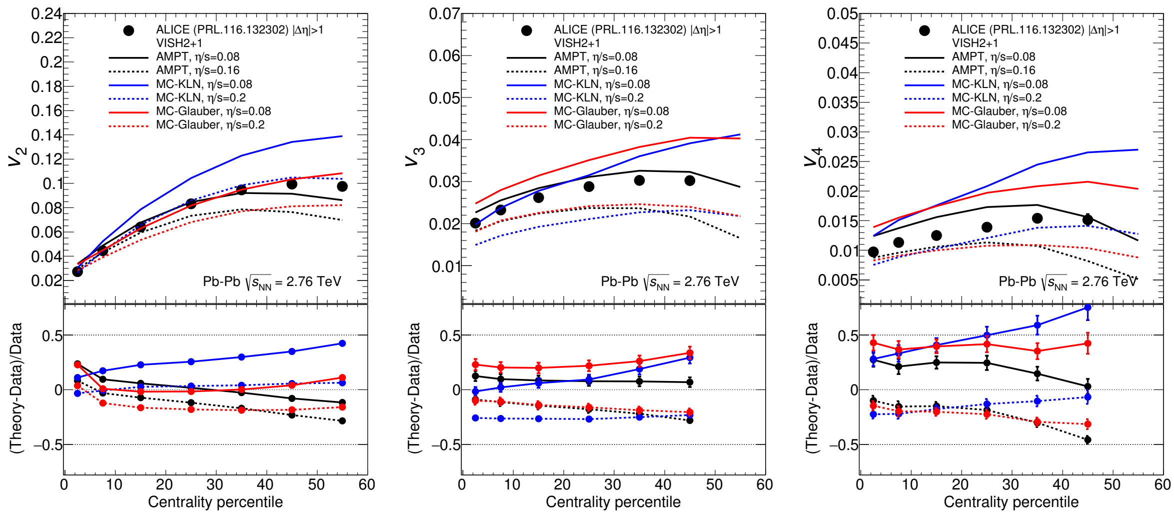

Fig. A.2: The individual flow harmonics v_n (n = 2, 3 and 4) in Pb–Pb collisions at $\sqrt{s_{\rm NN}} = 2.76$ TeV [3] are compared to various VISH2+1 calculations [42]. Three initial conditions from AMPT, MC-KLN and MC-Glauber are drawn as different colors. The η/s parameters are shown as different line styles, the small shear viscosity ($\eta/s = 0.08$) are shown as solid lines, and large shear viscosities ($\eta/s = 0.2$ for MC-KLN and MC-Glauber, 0.16 for AMPT) are drawn as dashed lines.

normalized symmetric cumulants (NSC(m,n)) quantitively for most centralities while the string melting AMPT model fails to describe them.

Finally, few selected calculations from three theoretical models which describe the v_n data best are shown in Fig. A.4. The calculations from event-by-event EKRT+viscous hydrodynamics, VISH2+1 with AMPT initial conditions (η/s = 0.08) and the string melting version of AMPT give the best description of the individual flow harmonics v_n (n = 2, 3 and 4) with an accuracy of 5-20%. The centrality dependence differs in the three models as well as in the different order flow harmonics. The simultaneous description of individual flow harmonics v_n at all orders is necessary to further optimize model parameters and put better constraints on the initial conditions and the transport properties of nuclear matter in ultra-relativistic heavy-ion collisions together with SC(m,n) and NSC(m,n).

B The ALICE Collaboration

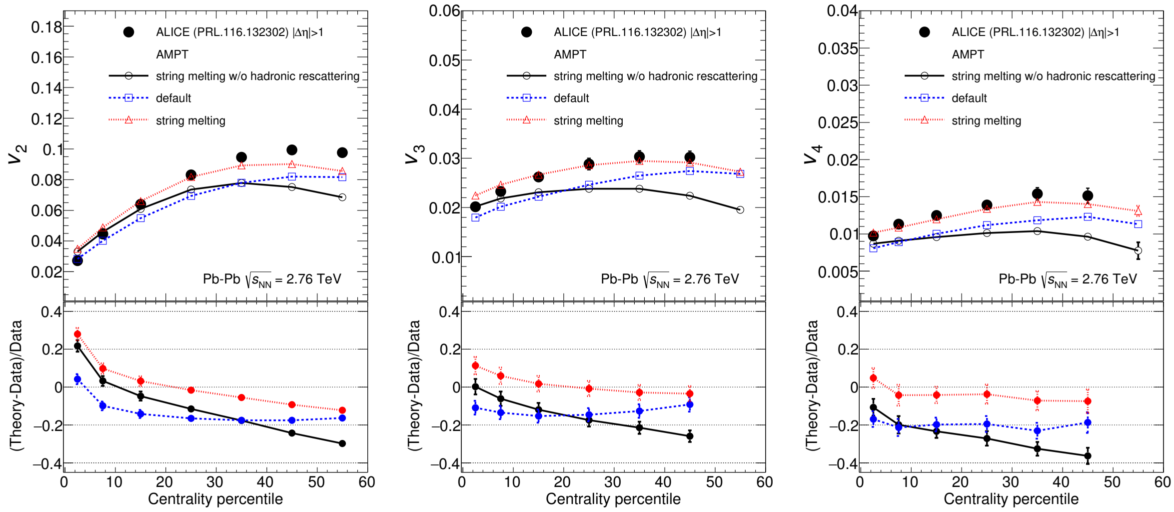

Fig. A.3: The individual flow harmonics v_n (n = 2, 3 and 4) in Pb–Pb collisions at $\sqrt{s_{\mathrm{NN}}}$ = 2.76 TeV [3] are compared to various AMPT models.

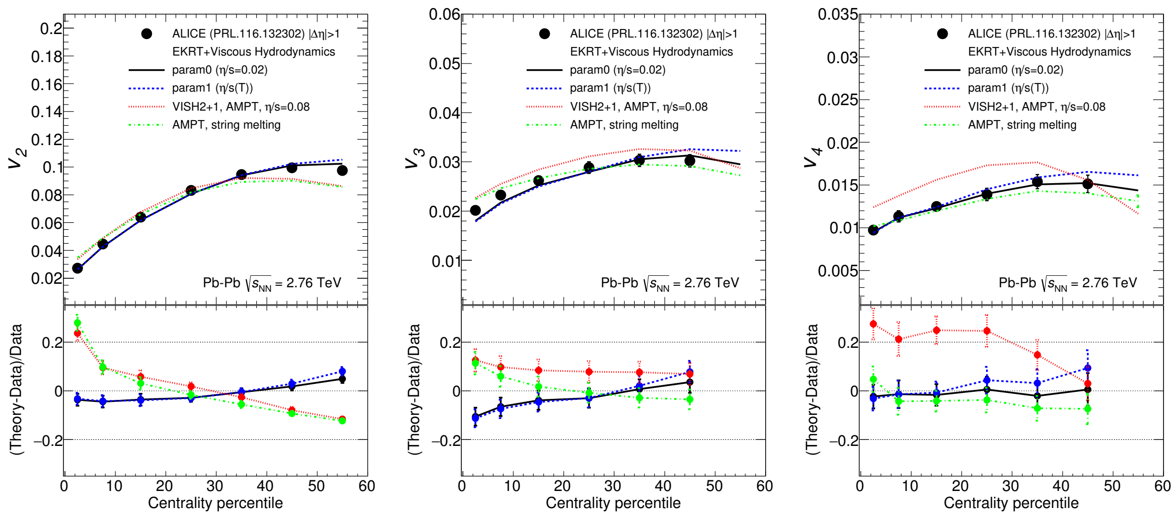

Fig. A.4: The individual flow harmonics v_n (n = 2, 3 and 4) in Pb–Pb collisions at $\sqrt{s_{\mathrm{NN}}}$ = 2.76 TeV [3] are compared to few selected model calculations from three theoretical models which describe the v_n data best.